NASA Contractor Report 185130
AIAA-89-2832

Plume Characteristics of MPD Thrusters: A Preliminary Examination

Roger M. Myers
Sverdrup Technology, Inc.
NASA Lewis Research Center Group
Cleveland, Ohio

September 1989

Prepared for
Lewis Research Center
Under Contract NAS3-25266

National Aeronautics and
Space Administration

PLUME CHARACTERISTICS OF MPD THRUSTERS: A PRELIMINARY EXAMINATION

Roger M. Myers*
Sverdrup Technology, Inc.
NASA Lewis Research Center Group
Cleveland, Ohio 44135

SUMMARY

A diagnostics facility for MPD thruster plume measurements has been built and is currently undergoing testing. The facility includes electrostatic probes for electron temperature and density measurements, Hall probes for magnetic field and current distribution mapping, and an imaging system to establish the global distribution of plasma species. Preliminary results for MPD thrusters operated at power levels between 30 and 60 kW with solenoidal applied magnetic fields show that the electron density decreases exponentially from 1×10^{20} m^{-3} to 2×10^{18} m^{-3} over the first 30 cm of the expansion while the electron temperature distribution is relatively uniform, decreasing from ~2.5 to 1.5 eV over the same distance. The radiant intensity of the ArII 4879 Å line emission also decays exponentially. Current distribution measurements indicate that a significant fraction of the discharge current is blown into the plume region, and that its distribution depends on the magnitudes of both the discharge current and the applied magnetic field.

INTRODUCTION

The potential for high specific impulse and system simplicity make MPD thrusters attractive for propulsion applications on planetary, orbit transfer, and maneuvering missions (refs. 1 and 2). However, demonstrated thruster efficiencies are still too low to make MPD thrusters practical for these applications. The goal of this research is to establish the performance limitations of these devices by examining the physical mechanisms of thruster energy deposition.

The physical processes which govern acceleration and internal energy deposition via ionization and propellant heating are distributed throughout the thruster and near field plume. Interelectrode electron densities measured in quasi-steady thruster (1 to 2 ms pulse) by Turchi (ref. 3) and Tahara (ref. 4) indicate that the primary ionization zone for argon propellant is near the thruster backplate. However, Bruckner (ref. 5) and Boyle (ref. 6), using optical and double electrostatic probe techniques, measured the exhaust velocity of self-field thrusters and found that significant acceleration took place in the first 15 cm outside the thruster. Maisenhalder (ref. 7) used rapidly rotating single electrostatic probes to establish flow streamlines, electron temperatures, and densities in the plume of a steady-state, self-field MPD thruster. Fradkin (ref. 8), using a Rogowski coil, showed that as much as 40 percent of the discharge current could flow more than 90 cm downstream of an applied field MPD thruster. These measurements indicate a substantial amount of energy deposition in the plume region, but are limited to high power quasi-steady or low power steady-state operation and to a narrow range of thruster operating conditions.

---

*Member AIAA.

The goal of this work is to establish the plasma characteristics and dominant physical processes present in the exhaust plume of both self and applied field steady-state MPD thrusters operated at power levels between 20 and 250 kW. Following an overview of the experimental facility, the plume diagnostic techniques and their implementation are presented. Preliminary measurements of the electron density and temperature, ionized argon line intensity and current distributions are shown and their implications discussed.

EXPERIMENTAL FACILITY AND THRUSTER CONFIGURATIONS

The MPD thruster test facility consisted of a 3 m diameter, 3 m long spool piece attached to a 21 m long, 7.6 m diameter vacuum tank via a 3 m diameter gate valve. Thrusters were mounted on a thrust stand within the spool piece, and the gate valve was opened to test the thrusters. The thruster support assembly is shown schematically in figure 1. The tank pressure was maintained at pressures below 0.07 Pa ($5x10^{-4}$ torr) during testing at argon flow rates up to 0.16 g/s. The thrusters were powered by four 66 kW welding supplies combined in a series/parallel circuit to give 88 V at 3000 A. A solenoidal magnetic field was applied using a 46 turn, 14 cm inner diameter, 15.2 cm long coil surrounding the thruster anode. A single welding supply was used to drive up to 1500 A through this magnet, generating a 0.2 tesla magnetic field at the cathode tip. Further details on the facility may be found in references 9 to 11.

The thruster configurations used for these experiments, shown in figure 2, used a cylindrical water cooled copper anode and a 2 percent thoriated tungsten cathode. The thruster designations (D, E, and F) correspond to those used in reference 10. Configuration D had a cylindrical anode which ended in a short, 41° flare. The continuously flared anode geometry used for geometries E and F was 5.4 cm long with a 10.5° half angle. For all thrusters the cathode diameter was 1.27 cm; its length was 2.2 cm for geometries D and E and 3.8 cm for geometry F. The primary chamber dimensions are listed in table I. Argon propellant was injected through the backplate.

DIAGNOSTICS

Electrostatic and Hall probes were used with a positioning system to study the electron density/temperature and current distributions and a charge injection device (CID) camera was used with narrow bandpass interference filters to establish global plasma species distributions. In this section detailed descriptions of these diagnostics are presented.

Probe System

The principal problem with intrusive diagnostics of high power steady-state plasma thrusters is the extremely hostile environment in which the measurements are made. Total enthalpies in the exhaust plume can reach up to $5x10^8$ J/kg. For this research the probes were swept through the plume in ~50 ms to avoid the large sizes associated with active cooling. The drive system, shown in figure 3, consisted of a stepper motor driven linear actuator used to move the probes axially on which a dc motor was mounted to rotate the probes through the plume. The probe arm length was such that the probes passed

directly through the thruster axis and a variable potentiometer was used to detect the angular position of the probe arm during the plume traverse. Data were acquired at 1 kHz during each pass through the plume. The entire motion and data acquisition sequence was controlled using a personal computer.

Electrostatic probes. - The rapid probe motion makes use of standard single and double probe techniques (ref. 12) difficult. For this reason the simpler triple probe technique developed by Chen (ref. 13), and recently implemented at the University of Stuttgart (ref. 14), was used for these experiments. This technique eliminates the requirement for a voltage ramp and permits rapid evaluation of the electron temperature and density. Comparisons of results from the triple probe method with double probe and nonintrusive interferometric techniques have shown good agreement under conditions similar to those expected in MPD thruster plumes (refs. 15 and 16). As shown in figure 4, the triple probe technique relies on applying a constant bias voltage between two probes while a third is allowed to electrically float nearby. The electron temperature, T_e, and density, N_e, are related to the floating voltage, V_{d2}, and the current, I_{d3}, by (ref. 13)

$$\frac{1}{2} = \frac{1 - \exp\left(\frac{-eV_{d2}}{kT_e}\right)}{1 - \exp\left(\frac{-eV_{d3}}{kT_e}\right)} \tag{1}$$

$$N_e = \frac{\exp(0.5) I_{d3} \left(\frac{m_i}{kT_e}\right)^{1/2}}{eA_p\left[\exp\left(\frac{eV_{d2}}{kT_e}\right) - 1\right]} \tag{2}$$

where the voltages are defined in figure 4 and A_p is the individual probe surface area. These relations are based on the assumptions of a Maxwellian electron distribution function, a collisionless probe sheath, and negligible inter-probe interaction. The latter requires that the probe separation be much larger than the Debye length. The probes are aligned with the thruster axis to minimize the impact of flow angle on the electron density measurements. This effect goes to zero along the axis (where the probes are in line with the flow), and the axial variation in the shape of the electron density distribution implies this effect introduces an error of less than 20 percent at the largest axial/radial position examined (worst case). The impact of the magnetic field on the probe measurements should be small for the conditions studied (ref. 13).

The triple electrostatic probe consisted of three 0.25 mm diameter, 1 cm long, tungsten wires each separated by 1 mm. Probe end effects (ref. 17) should be small for this geometry (length to diameter ratio, ~50). Alumina tubes, which were 1.4 mm in diameter and 3.8 cm long, were used as the insulators. A constant bias (V_{d3}) of 17 V was applied using a 30 V, 2 A power supply. Testing revealed that varying V_{d3} between 6 and 18 V had little impact on the measurements. All signals were sent through isolation amplifiers (3 dB

point at 10 kHz) before going to the data acquisition system. Repeated rotations through the plume at constant axial position showed no change in the probe signals indicating that probe contamination was not significant.

Hall probes. - The current distribution was measured by rotating a Hall effect transducer through the plume. Assuming an azimuthally symmetric current distribution, the self-induced magnetic field distribution is related to the enclosed current, J_{enc}, by

$$B_\theta(r) = \frac{\mu_o J_{enc}(r)}{2\pi r} \tag{3}$$

where the assumption of symmetry can be checked a posteriori. As shown in figures 2 and 5, the probe orientation during the traverse is such that its response is given by

$$B_p = B_r \sin\theta + B_\theta \cos\theta \tag{4}$$

where B_p is the field measured by the probe, B_r is the radial field component due to the applied field and θ is the angle between the probe and the local radius, r_p. From figure 5 it is apparent that θ is equal to one-half the angle between the probe arm and the local vertical. The contribution from B_r is largest at the largest radius (where both θ and B_r are largest). Assuming current does not extend radially outside the thruster (which can again be checked a posteriori), the maximum radius is the thruster radius, r_t, so that

$$B_p = B_r \sin\left(\frac{r_t}{2R_p}\right) + B_\theta \sqrt{1 - \left(\frac{r_t}{2R_p}\right)^2} \tag{5}$$

where R_p is the length of the probe arm. For the dimensions given in figures 2 and 5 this results in the inequality

$$B_r < 4B_\theta \tag{1}$$

for the B_r term to contribute less than 10 percent of the measured value. To establish minimum measurable currents the radial field distribution was calculated using a thick, finite length solenoid code (ref. 18). Typical results are shown in figure 6 for $z = 2.7$ cm and three magnet current levels. For each magnetic field strength the minimum measurable B_θ is established using equation (6).

The dependence of Hall probe output on temperature is shown in figure 7. A 50 °C temperature increase decreased the sensor output by ~8 percent. To minimize the impact of probe heating during the plume traverse a 0.5-mm-thick mica sheet was placed on either side of the probe and the edges were sealed with ceramic cement. In addition, a thermocouple was located immediately beside the probe to monitor its temperature during thruster operation. Preliminary testing revealed that while the probe temperature did not increase significantly during the passage through the plume, prolonged exposure, even while far outside the main plume, increased its temperature by over 100 °C. For this reason a small water cooling line was passed up through the probe arm. High

thermal conductivity epoxy was used to conduct heat from the probe back to the arm. In this fashion the sensor temperature was kept constant without sacrificing the small probe size.

Filter photography. - A CID camera was used with narrow bandpass optical interference filters to study global plasma species distributions. The camera was mounted perpendicularly to the thruster axis to image the near field plume. The distribution of the 4p ionized argon quantum state was examined by observing the 4879 Å line emission with a filter bandpass of 10 Å. Images were directly digitized using a frame grabber and commercial software. At this stage of the research no Abel-inversion was performed.

PRELIMINARY RESULTS

The MPD thrusters were operated at current levels between 1000 and 1500 A at an argon mass flow rate of 0.16 g/s. The solenoid current was varied between 400 and 1500 A. Voltage-current characteristics and performance measurements are reported in reference 10.

Electron density and temperature profiles for thrust F at several axial positions downstream of the exit plane are shown in figures 8(a) and (b). These data were obtained at a discharge current, Jt, of 1500 A, magnet current, Jm, of 800 A and a mass flow rate of 0.16 g/s ($J^2/\dot{m} = 1.4 \times 10^{10}$ $A^2 \cdot s/kg$). The triple probe technique fails for electron number densities below 10^{16} m^{-3} because of probe sheath interactions at low densities. It is clear that while electron temperature exhibited strong radial gradients near the exit plane (reaching a peak over 2.5 eV on centerline), its axial variation was gradual. The electron density, however, decayed rapidly in both radial and axial directions. Shown in figure 9 is a plot of the centerline electron density versus axial position and the associated least-squares curve fit. Starting from $\sim 1 \times 10^{20}$ m^{-3}, the decay is exponential at a constant rate over the first 30 cm of the plume. These results are similar to those obtained by Arakawa (ref. 19) using a permanent magnet applied field with a 10 kW thruster ($J^2/\dot{m} = 4.4 \times 10^{10}$ $A^2 \cdot s/kg$), though the axial decay rates observed in this work are lower. The different decay rates are probably due to the different shapes of the applied fields used in the two experiments.

The influence of the applied magnetic field on the density and temperature at $z = 22$ cm is shown in figures 11(a) and (b). The applied field strength had little impact on the electron temperature at this axial position, but the peak electron density decreased by ~30 percent and its radial extent increased slightly at lower field strengths. The ratio of the gas to magnetic pressure, defined by

$$\beta = \frac{\Sigma NkT}{B^2/2\mu_o} \tag{7}$$

was evaluated using the calculated axial field strengths and assuming $N_i = N_e$ and $T_e = T_i$. Results for a solenoid current of 800 A are shown in figure 10. β increased exponentially with axial distance from 0.02 at $z = 1$ cm to 0.35 at $z = 30$ cm. It is apparent from these results that the magnetic field significantly confined the plasma in the near field expansion.

The intensity decay rates for the 4879 Å, ArII line for solenoid current levels of 1500 and 800 A are shown in figure 12. For both cases the detector was saturated at an intensity of 255 near the exit plane. Increasing the magnetic field strength increased the intensity of the emission at a given axial location, indicating a corresponding increase in the population of the upper excited state. Least-squares curve fits reveal that the axial intensity, which is directly proportional to the density of the upper excited state, decayed exponentially for both magnetic field strengths, though there was a slight increase in rate for $z > 3$ cm. The least-squares fits were very close for both magnetic field strengths, with the equation

$$I = I_o \exp\left(\frac{-z}{2.3}\right) \qquad (z \text{ in cm}) \tag{8}$$

describing both curves. From this result it is apparent that the characteristic length for decay was ~2.3 cm. Using the radiative lifetime for this state (ref. 20) (1.3×10^{-8} s) and an exhaust velocity of ~10^4 m/s (justified by thrust measurements (ref. 8)), the expected decay length is 0.01 cm, which is two orders-of-magnitude smaller than the observed length. These estimates indicate there is either significant collisional excitation or ArIII - ArII recombination during the expansion, especially since the calculation does not account for radial plume expansion. The recombination rate was evaluated using the cross sections given by Drawin (ref. 21) and was found to be several orders-of-magnitude too small to explain the data. It is thus expected that electronic excitation plays a dominant role in the near field plume.

Results of the Hall probe enclosed current measurements for thruster geometry D are shown in figures 13(a) and (b) for $z = 2.7$ cm for two magnet currents at a discharge current of 1500 A and argon flow rate of 0.16 g/s. The maximum enclosed current occurred at a radius equal to the anode exit radius, indicating most of the current blown into the plume attached to the face of the anode. Comparison of the two figures indicates that the fractional current blown downstream of this axial position increases with magnet current. For magnet and thruster current equal to 1500 A, over 30 percent of the discharge current was blown downstream of 3 cm.

These measurements have helped explain the temporal variation of the voltage observed under certain operating conditions (ref. 8). For these cases the voltage increased monotonically with time with no change in thruster current, mass flow rate, or applied field strength. As shown in figure 14, the Hall probe measurements clearly show that a change in current distribution was associated with the change in voltage with more current blown downstream when the thruster operates at a higher voltage. The increased path length for the current streamlines will increase the discharge voltage in agreement with the observations. While the causes of the current redistribution are still unknown, these measurements indicate that the voltage increase was not associated with an electrode fall voltage.

The results presented in this section indicate that a significant amount of energy transfer occurs in the plume. The fact that a significant fraction of the thruster current was blown downstream implies not only that there was ohmic heating in the plume, but also that the interaction volume between the applied field and the discharge current had increased. In addition, the applied magnetic field appears to confine the plume expansion which, by

decreasing axial electron density gradients, increases the collision frequencies and enhances electron-ion equilibration. In fact, the electron-ion equilibration time for the measured densities and temperatures is $\sim 10^{-5}$ sec, which for a velocity of 10^4 m/s yields an equilibration length of 10 cm which is comparable to the length scales of the density decay.

SUMMARY

An MPD thruster plume diagnostics facility, including electrostatic probes for electron density and temperature measurements, Hall probes for current distribution mapping, and an imaging system to establish global plasma species distributions has been built and is undergoing testing. Preliminary measurements indicate that for applied field MPD thrusters operated at powers between 30 and 60 kW the electron density distribution is strongly peaked along the centerline and decays exponentially with axial distance from the thruster exit plane. The electron temperature distribution is more uniform, dropping from ~2.5 eV at the exit to ~1.5 eV at a distance 30 cm downstream. These results, combined with calculated applied field distributions, indicate significant plasma confinement and energy transfer in the plume.

ACKNOWLEDGMENTS

The author thanks Mark Vernyi and Dave Wehrle for their help with the construction of the probes and motion system, and Dave Hoffmann and all the Tank 6 crew for their help in facility assembly and maintenance.

REFERENCES

1. Sovey, J.S.; and Mantenieks, M.A.: Performance and Lifetime Assessment of MPD Arc Thruster Technology. AIAA Paper 88-3211, July 1988 (NASA TM-101293).

2. Buhler, R.: Plasma Propulsion for Near Earth Missions of Large Space Structures. Inst. for Raumfahrtantriebe, University of Stuttgart, W. Germany, May 1984.

3. Turchi, P.: The Cathode Region of a Quasi-Steady Magnetoplasmadynamic Arcjet. Ph.D. Thesis, Princeton University, 1970.

4. Kagaya, Y., et al.: Experimental and Theoretical Researches on Arc Structure in a Self-Field Thruster. AIAA Paper 87-1093, May 1987.

5. Bruckner, A.: Spectroscopic Studies of the Exhaust of a Quasi-Steady MPD Accelerator. Ph.D. Thesis, Princeton University, May 1972.

6. Boyle, M.: Acceleration Processes in the Quasi-Steady Magnetoplasmadynamic Discharge. Ph.D. Thesis, Princeton University, 1974.

7. Maisenhalder, F.; and Mayerhofer, W.: Jet-Diagnostics of a Self-Field Accelerator with Langmuir Probes. AIAA J., vol. 12, no. 9, Sept. 1974, pp. 1203-1209.

8. Fradkin, D.: Analysis of Acceleration Mechanisms and Performance of an Applied Field MPD Arcjet. Ph.D. Thesis, Princeton University, 1973.

9. Sovey, J., et al.: Test Facility and Preliminary Performance of a 100 kW Class MPD Thruster. NASA TM-102021, 1989.

10. Mantenieks, M., et al.: Performance of a 100 kW Class Applied Field MPD Thruster. AIAA Paper 89-2710, July 1989 (NASA TM-102312).

11. Haag, T.: Design of a Thrust Stand for High Power Electric Propulsion Devices. AIAA Paper 89-2829, July 1989.

12. Swift, J.D.; and Schwar, M.J.R.: Electrical Probes for Plasma Diagnostics, Elsevier, 1970.

13. Chen, S.L.; and Sekiguchi, T.: Instantaneous Direct-Display System of Plasma Parameters by Means of Triple Probe. J. Appl. Phys., vol. 36, no. 8, Aug. 1965, pp. 2363-2375.

14. Auweter-Kurtz, M.: Personal Communication, University of Stuttgart, Oct. 1988.

15. Lenoci, M.; and Haas, G.: Investigation of the Parameters in the Boundary Plasma of ASDEX by Means of a Langmuir Probe. Max-Planck Inst. for Plasma Physick, Munich, Germany, July 1986.

16. Fischer, E., et al.: MPD Arcs as Plasma Sources for Recombination Lasers. Appl. Phys. B, vol. 38, no. 2, Oct. 1985, pp. 79-89.

17. Chung, P., Talbot, L.; and Touryan, K.J.: Electric Probes in Stationary and Flowing Plasmas. Springer-Verlag, 1976.

18. LaPointe, M.: Personal Communication, Sverdrup Technology, NASA LeRC Group, May 1989.

19. Arakawa, Y.; and Sasoh, A.: Steady-State Permanent Magnet Magnetoplasma-dynamic Thruster. J. Propulsion Power, vol. 5, no. 3, May-June 1989, pp. 301-304.

20. Wiese, W.L.; Smith, M.W.; and Miles, B.M.: Atomic Transition Probabilities, Sodium Through Calcium. NSRDS-NBS-22-Vol-2, National Bureau of Standards, 1969.

21. Drawin, H.W.: Collision and Transport Cross-Sections. EUR-CEA-FC--383 (Rev), 1967.

TABLE I. - MPD THRUSTER DIMENSIONS

Thruster designations	Anode channel diameter, mm	Channel length,[a] cm	Anode flare	
			Half angle, deg	Length, cm
D	26	[b]4.2	41	1.1
E	[c]26	[b]5.4	10.5	5.4
F	[c]26	[d]5.4	10.5	5.4

[a]Upstream end of cathode to anode exit plane.
[b]Cathode diameter 1.27 cm, cathode length 2.2 cm.
[c]Inlet diameter.
[d]Cathode diameter 1.27 cm, cathode length 3.8 cm.

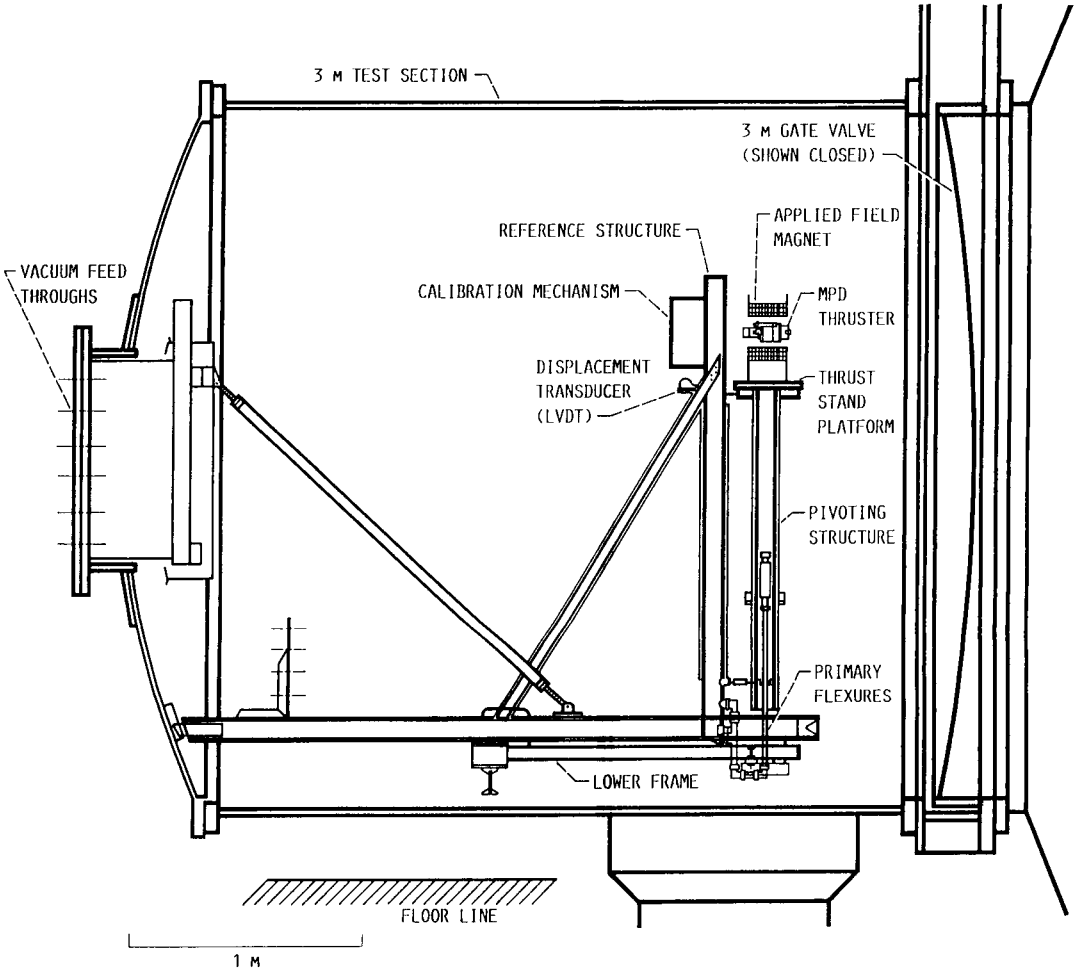

FIGURE 1. - SCHEMATIC OF THRUSTER SUPPORT AND THRUST STAND.

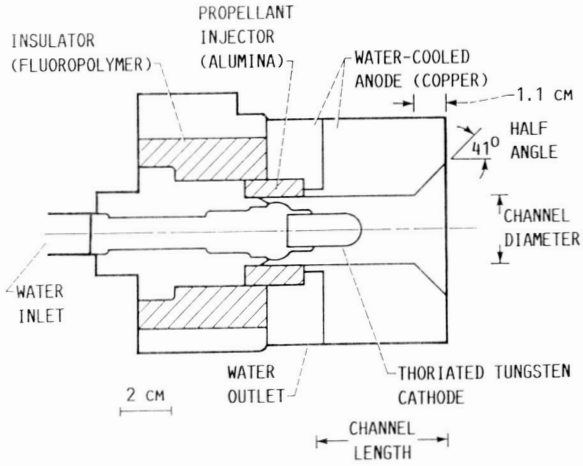

(A) CONFIGURATION D.

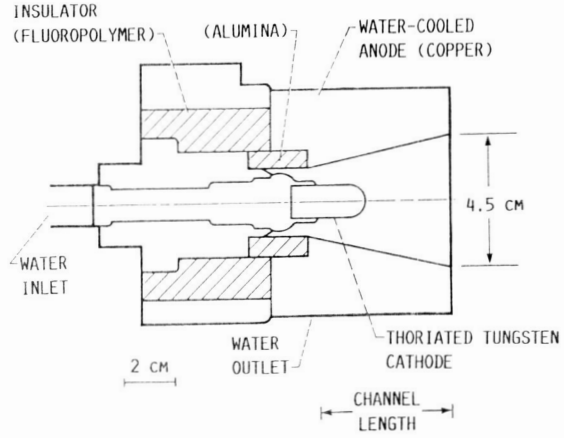

(B) CONFIGURATIONS E AND F.

FIGURE 2. - MPD THRUSTER CONFIGURATIONS (SEE TABLE 1).

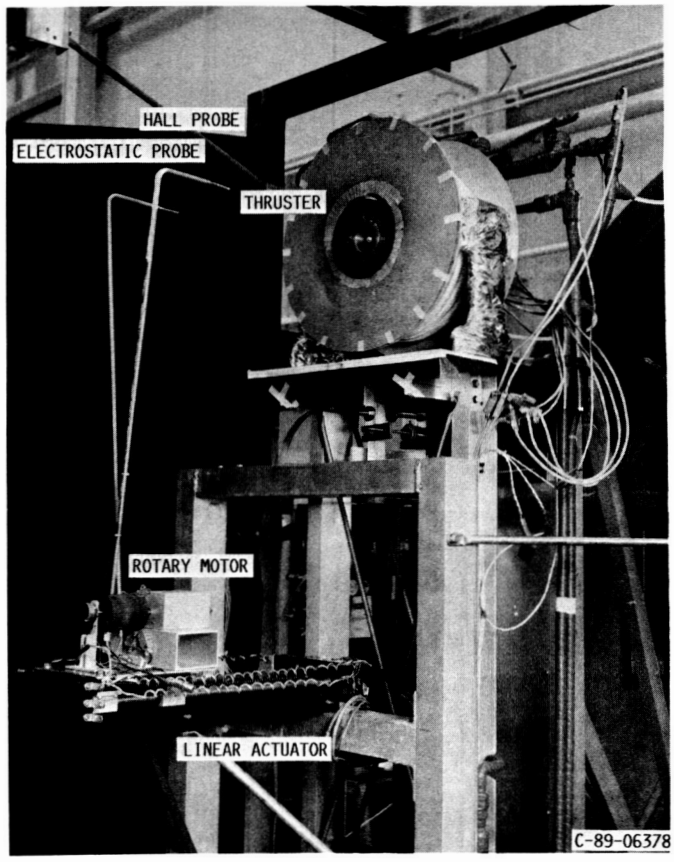

FIGURE 3. - PROBES AND MOTION SYSTEM.

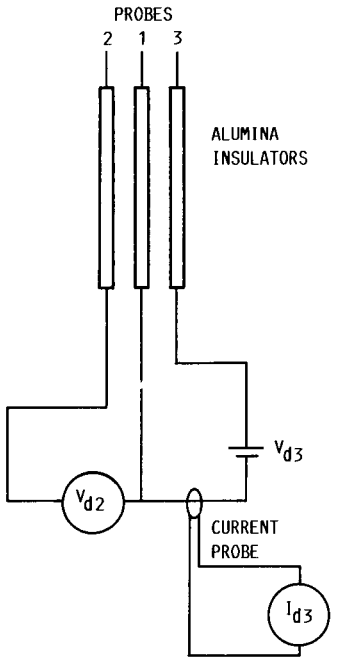

FIGURE 4. - TRIPLE PROBE CIRCUIT SCHEMATIC.

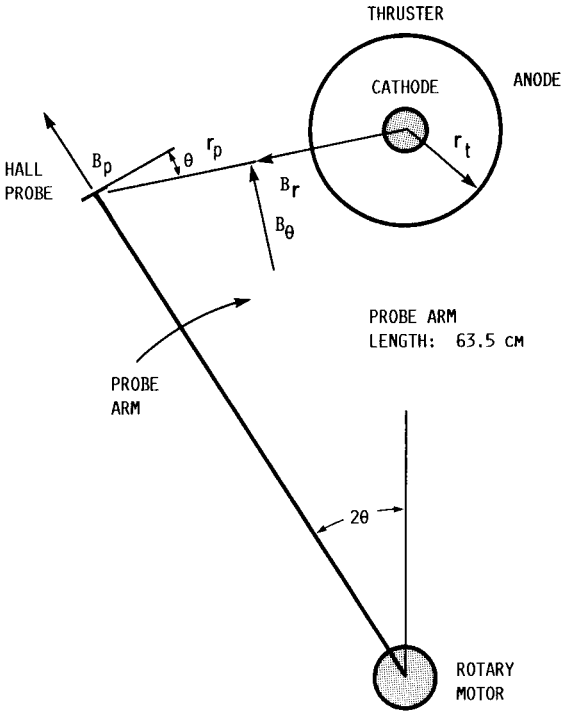

FIGURE 5. - GEOMETRIC CONFIGURATION OF HALL PROBE DIAGNOSTIC.

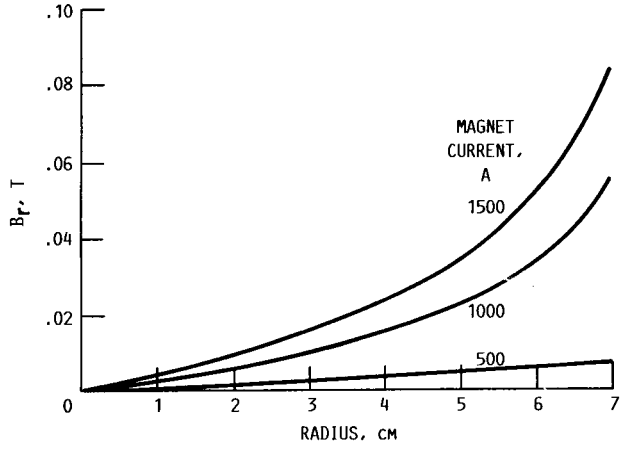

FIGURE 6. - CALCULATED RADIAL MAGNETIC FIELD DISTRIBUTION AT THE EXIT PLANE FOR 3 SOLENOID CURRENTS, z = 2.7 cm.

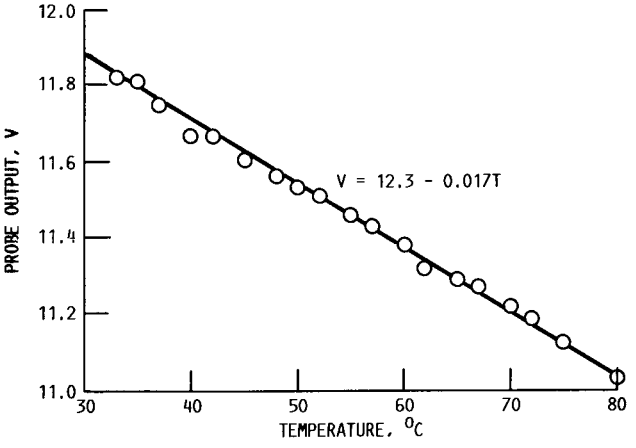

FIGURE 7. - HALL PROBE OUTPUT VOLTAGE DEPENDENCE ON TEMPERATURE, B = 0.3 TESLA.

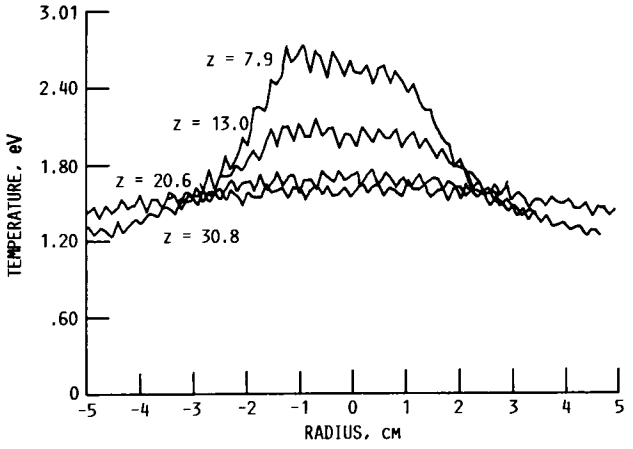

(a) ELECTRON TEMPERATURE.

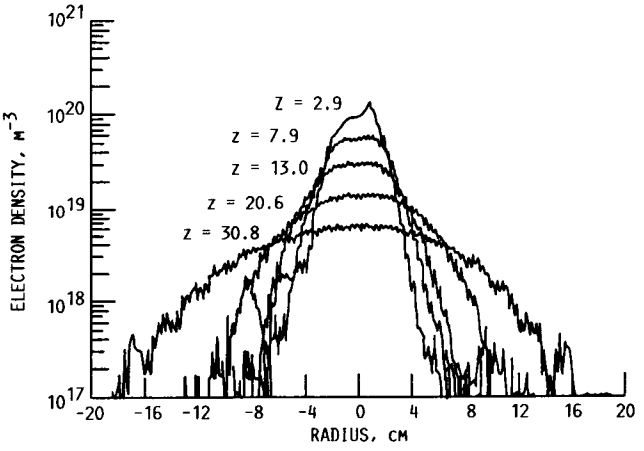

(b) ELECTRON DENSITY.

FIGURE 8. - PROFILES FOR SEVERAL AXIAL POSITIONS. (J_M = 800 AMPS, J_T = 1000 AMPS, $\dot{M}$ = 0.16 g/s).

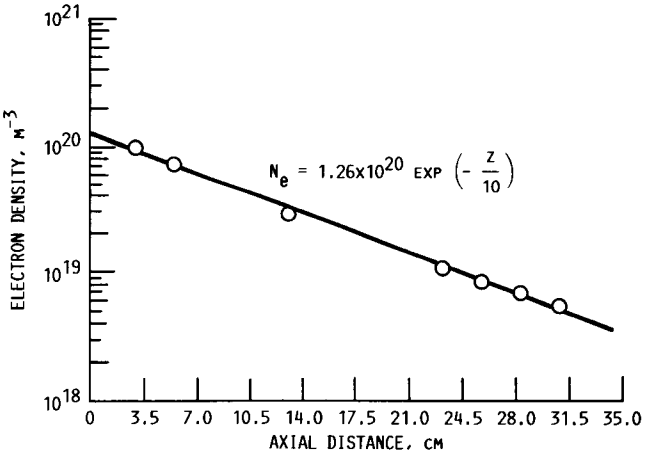

FIGURE 9. - CENTERLINE ELECTRON DENSITY VERSUS AXIAL POSITION. (J_M = 800 AMPS, J_T = 1000 AMPS, $\dot{M}$ = 0.16 g/s).

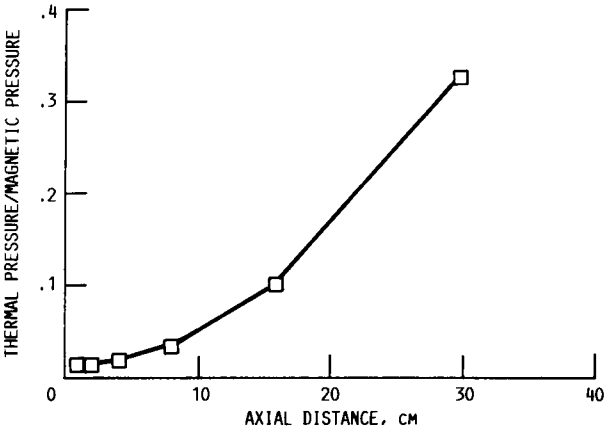

FIGURE 10. - RATIO OF THERMAL TO MAGNETIC PRESSURE ALONG PLUME AXIS, DATA FROM FIGURE 9.

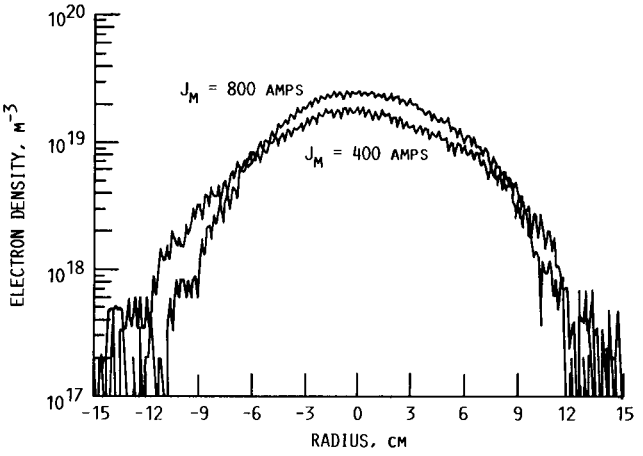

(a) ELECTRON DENSITY.

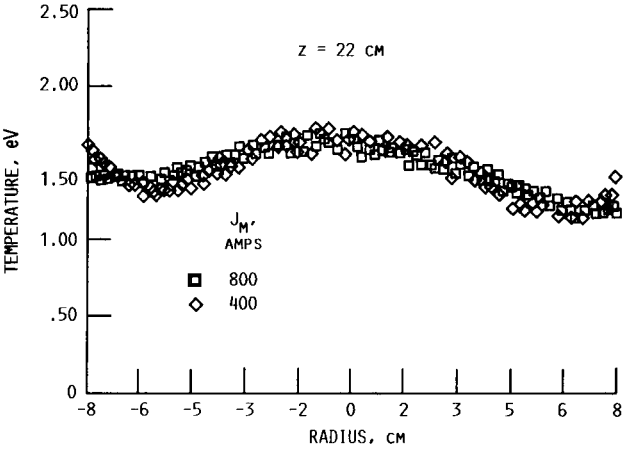

(b) ELECTRON TEMPERATURE.

FIGURE 11. - INFLUENCE OF APPLIED FIELD STRENGTH ON PROFILE AT z = 22 CM, J_T = 1000 AMPS, $\dot{M}$ = 0.16 g/s.

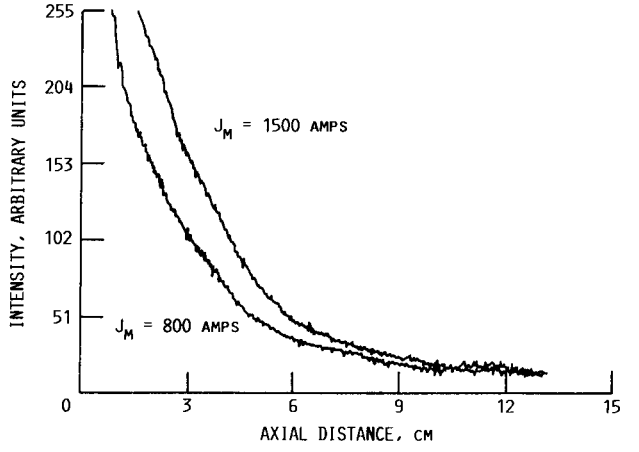

FIGURE 12. - CENTERLINE INTENSITY DISTRIBUTION FOR SINGLY IONIZED ARGON 488 NM LINE EMISSION, J_T = 1500 AMPS, $\dot{M}$ = 0.16 g/s.

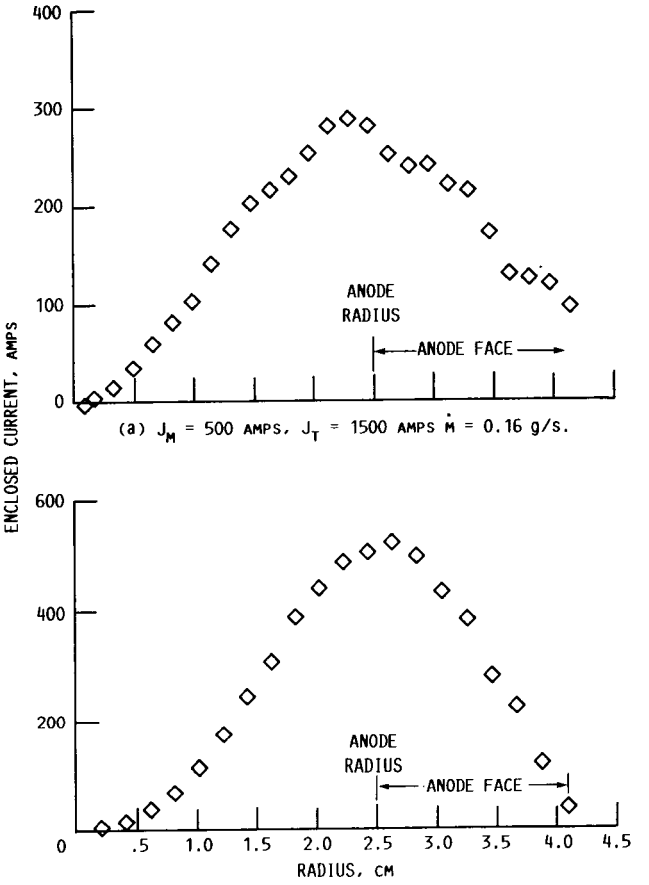

(a) J_M = 500 AMPS, J_T = 1500 AMPS $\dot{M}$ = 0.16 g/s.

(b) J_M = 1500 AMPS, J_T = 1500 AMPS, $\dot{M}$ = 0.16 g/s.

FIGURE 13. - ENCLOSED CURRENT DISTRIBUTION AT z = 2.7 CM.

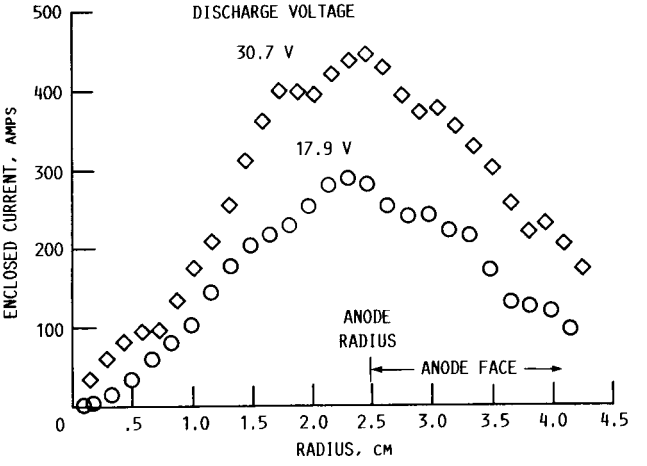

FIGURE 14. - ENCLOSED CURRENT DISTRIBUTIONS SHOWING CHANGE CAUSING VOLTAGE DIFFERENCE, J_M = 423 AMPS, J_T = 1500 AMPS, $\dot{M}$ = 0.16 g/s.

NASA
National Aeronautics and Space Administration

Report Documentation Page

1. Report No.	2. Government Accession No.	3. Recipient's Catalog No.
NASA CR-185130 AIAA-89-2832		

4. Title and Subtitle	5. Report Date
Plume Characteristics of MPD Thrusters: A Preliminary Examination	September 1989
	6. Performing Organization Code

7. Author(s)	8. Performing Organization Report No.
Roger M. Myers	None (E-5018)
	10. Work Unit No.
	506-42-31
9. Performing Organization Name and Address	11. Contract or Grant No.
Sverdrup Technology, Inc. NASA Lewis Research Center Group Cleveland, Ohio 44135	NAS3-25266
	13. Type of Report and Period Covered Contractor Report Final
12. Sponsoring Agency Name and Address	14. Sponsoring Agency Code
National Aeronautics and Space Administration Lewis Research Center Cleveland, Ohio 44135-3191	

15. Supplementary Notes

Project Manager, James S. Sovey, Space Propulsion Technology Division, NASA Lewis Research Center. Prepared for the 25th Joint Propulsion Conference cosponsored by the AIAA, ASME, SAE, and ASEE, Monterey, California, July 10-12, 1989.

16. Abstract

A diagnostics facility for MPD thruster plume measurements has been built and is currently undergoing testing. The facility includes electrostatic probes for electron temperature and density measurements, Hall probes for magnetic field and current distribution mapping, and an imaging system to establish the global distribution of plasma species. Preliminary results for MPD thrusters operated at power levels between 30 and 60 kW with solenoidal applied magnetic fields show that the electron density decreases exponentially from 1×10^{20} to 2×10^{18} m^{-3} over the first 30 cm of the expansion, while the electron temperature distribution is relatively uniform, decreasing from approximately 2.5 eV to 1.5 eV over the same distance. The radiant intensity of the ArII 4879 Å line emission also decays exponentially. Current distribution measurements indicate that a significant fraction of the discharge current is blown into the plume region, and that its distribution depends on the magnitudes of both the discharge current and the applied magnetic field.

17. Key Words (Suggested by Author(s))	18. Distribution Statement
MPD thrusters Plasma diagnostics Electric propulsion Plume phenomena	Unclassified – Unlimited Subject Category 20

19. Security Classif. (of this report)	20. Security Classif. (of this page)	21. No of pages	22. Price*
Unclassified	Unclassified	16	A03

NASA FORM 1626 OCT 86

*For sale by the National Technical Information Service, Springfield, Virginia 22161